Drug Delivery Hot Paper

International Edition: DOI: 10.1002/anie.201508626
German Edition: DOI: 10.1002/ange.201508626

Engineering Polymer Hydrogel Nanoparticles for Lymph Node-Targeted Delivery

Stefaan De Koker[+], Jiwei Cui[+], Nane Vanparijs[+], Lorenzo Albertazzi, Johan Grooten, Frank Caruso, and Bruno G. De Geest**

Abstract: *The induction of antigen-specific adaptive immunity exclusively occurs in lymphoid organs. As a consequence, the efficacy by which vaccines reach these tissues strongly affects the efficacy of the vaccine. Here, we report the design of polymer hydrogel nanoparticles that efficiently target multiple immune cell subsets in the draining lymph nodes. Nanoparticles are fabricated by infiltrating mesoporous silica particles (ca. 200 nm) with poly(methacrylic acid) followed by disulfide-based crosslinking and template removal. PEGylation of these nanoparticles does not affect their cellular association in vitro, but dramatically improves their lymphatic drainage in vivo. The functional relevance of these observations is further illustrated by the increased priming of antigen-specific T cells. Our findings highlight the potential of engineered hydrogel nanoparticles for the lymphatic delivery of antigens and immune-modulating compounds.*

Modulating T and B cell immunity not only is key to the development of improved and new vaccines against pathogens, but also holds great promise to treat malignancies, autoimmune diseases, and allergies.[1,2] Priming of T cell responses requires the presentation of antigens, in the format of processed peptide fragments loaded onto major histocompatibility complexes, by dendritic cells (DCs). Priming of B cells and their differentiation into antibody secreting plasma cells relies on surface triggering of the B cell receptor (BCR) by antigens. Previous studies have shown that the priming of naïve T and B cells can be dramatically enhanced by delivering antigens formulated as nano- or microparticles.[1–6] Compared to soluble antigens, particulate vaccines enhance the quality and the magnitude of the adaptive immune response by acting on different levels. At the level of the DC, they increase antigen uptake and improve antigen presentation to T cells qualitatively and quantitatively. Peptide fragments of particulate antigens are loaded onto MHCII and MHCI molecules and thus can evoke both CD4 and CD8 T cell responses. By contrast, soluble antigens are almost exclusively presented via MHCII molecules, resulting in an immune response restricted to CD4 T cells. At the level of the B cell, the display of multiple antigen copies at the particle surface dramatically increases activation of B cells by simultaneous triggering of multiple BCRs on the B cell surface.[7]

T cell and B cell priming exclusively occur in secondary lymphoid organs. As a consequence, the efficacy with which vaccine carriers reach these sites constitutes a critical determinant of their efficacy to induce adaptive immunity and thus ultimately affects the protective efficacy of the vaccine.[8–11] As vaccines are commonly delivered by intramuscular or subcutaneous injection, lymph nodes are the lymphoid organs vaccines need to target. To move from the site of injection to lymph nodes, vaccines must be either transported actively to the lymph nodes by tissue DCs or they need to move along the interstitial flow, across the extracellular matrix, into the lymphatics.[12] As the latter process does not involve cellular uptake for transport, it is called passive drainage. The way particles drain to lymph nodes, and the efficacy with which they reach antigen-presenting cells, mainly depends on their in situ mobility after injection. Particles that show limited mobility in the extracellular matrix rely on local DCs recruited to the injection site for uptake and transport. Such particles become surrounded by fibrous tissue and become engulfed predominantly by tissue macrophages. As a consequence, only a minor fraction of particle-delivered antigens will reach the lymph nodes and contribute to the induction of the antigen-specific immune response. Moreover, the long-term presence of particles at the injection site creates an antigen depot that could cause exhausted T cell responses, and could hamper vaccine elicited protection.[13,14] In contrast, particles with high mobility in the extracellular matrix can move along the interstitial flow and thus have better potential to reach the lymph nodes, either after uptake by tissue DCs or after passive entry into the lymphatics. Similar requirements are needed for nanomaterial-based sentimental lymph node mapping.[15]

[*] Dr. S. De Koker,[+] N. Vanparijs,[+] Prof. B. G. De Geest
Department of Pharmaceutics, Ghent University
Ghent (Belgium)
E-mail: br.degeest@ugent.be
Dr. S. De Koker,[+] Prof. J. Grooten
Department of Biomedical Molecular Biology
Ghent University, Ghent (Belgium)
Dr. J. Cui,[+] Prof. F. Caruso
ARC Centre of Excellence in Convergent Bio-Nano Science and Technology, Department of Chemical and Biomolecular Engineering
The University of Melbourne, Parkville, Victoria (Australia)
E-mail: fcaruso@unemelb.edu.au
Dr. L. Albertazzi
Institute for Complex Molecular Systems and
Laboratory of Chemical Biology
Eindhoven University of Technology
Eindhoven (The Netherlands)
Dr. L. Albertazzi
Institute for Bioengineering of Catalonia (IBEC)
Barcelona (Spain)
[+] These authors contributed equally to this work.

Supporting information for this article, including experimental details, is available on the WWW under http://dx.doi.org/10.1002/anie.201508626.

However, there is much debate on the size and physicochemical properties of particles required to ensure optimal lymph node targeting and often particle uptake in vitro is a poor predictor of in vivo particle mobility. In this context, PEGylation [i.e., surface modification with poly(ethylene glycol)] might improve the mobility of nanocarriers in the extracellular matrix following subcutaneous injection. PEGylation has shown to be a successful strategy to increase the half-life of proteins and nanoparticles in systemic circulation after intravenous injection by reducing the interaction with macrophages and serum proteins.[16] Here, we address the impact of PEGylation on the lymphatic drainage properties of reduction-sensitive hydrogel nanoparticles and its influence on the subsequent priming of T cells.

Mesoporous silica (MS) nanoparticles with an average size of 200 nm were synthesized according to a previously reported method.[17,18] Hydrogel nanoparticles are fabricated by infiltrating amine-modified MS nanoparticles with pyridine dithioethylamine (PDA-) modified poly(methacrylic acid) (PMA^{PDA}). Subsequently, cysteamine (SH-) modified poly(methacrylic acid) (PMA^{SH}) is infiltrated, leading to crosslinking by disulfide exchange (Figure 1).[19] To track

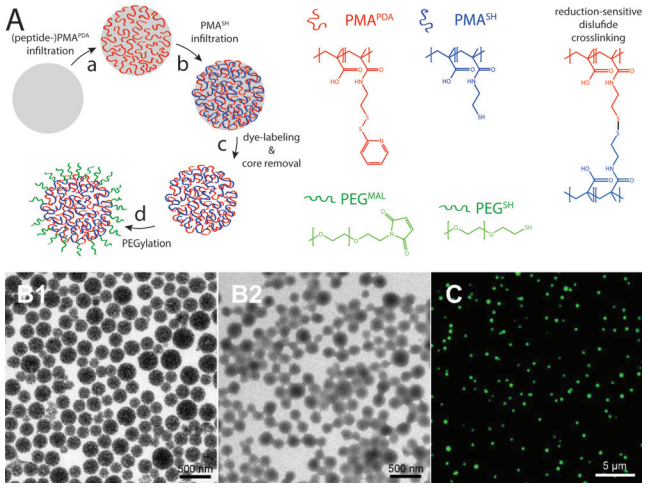

Figure 1. A) Schematic representation of the assembly of hydrogel nanoparticles. a) Infiltration of MS templates (ca. 200 nm) with PMA^{PDA}. b) Crosslinking of the PMA^{PDA} by infiltration of PMA^{SH} and disulfide exchange. c) Template dissolution. In the case of non-PEGylated nanoparticles, step (d) is omitted. d) PEGylation with PEG^{MAL} by thioether formation. B) TEM images of (B1) MS templates and (B2) PMA nanoparticles. C) Fluorescence microscopy image of AF488-labeled nanoparticles.

particle uptake, fluorescent labeling was performed with Alexa Fluor 488-cadaverine (AF488) prior to dissolution of the silica template particles in buffered HF solution. Since there are both residual thiols and pyridyldisulfides remaining in the PMA nanoparticles, PEGylation was performed by grafting maleimide-functionalized poly(ethylene glcyol) (PEG^{MAL}) and thiol-functionalized PEG (PEG^{SH}) onto the PMA nanoparticles. Figure 1B shows transmission electron microscopy (TEM) images of the MS template nanoparticles and the resulting PMA nanoparticles, and a fluorescence microscopy image of the nanoparticles. The TEM images demonstrate the porous nature of the silica templates and a similar diameter compared to the original MS templates. Dynamic light scattering (DLS) confirms the TEM data, showing an average particle size of 200 nm (polydispersity index, PDI: 0.07) for the MS templates and 185 nm (PDI: 0.1) for the PMA nanoparticles in a hydrated state (see Figure S1 in the Supporting Information). Also note that PEGylation does not significantly alter the size and morphology of the nanoparticles. The fluorescence microscopy image in Figure 1C shows that the PMA nanoparticles are well-dispersed in aqueous solution. By counting the nanoparticles by flow cytometry and measuring the fluorescence of a nanoparticle suspension by fluorimetry (Figure S2) we verified that both PMA and PEG-PMA nanoparticles bear similar fluorescence.

To investigate the interaction between the hydrogel nanoparticles and DCs in vitro, we incubated DCs with PMA and PEG-PMA nanoparticles followed by confocal microscopy and quantitative analysis using flow cytometry (FACS). Confocal microscopy of (Figure 2A) the cell membrane stained by AlexaFluor647-conjugated cholera toxin subunit B (AF647-CTB) demonstrated massive internalization of the nanoparticles by DCs. No obvious differences in cell interaction between both types of nanoparticles were observed from these images. Figure 2B shows flow cytometry data in terms of the percentage of nanoparticle-associated cells and their mean fluorescence. Nanoparticle uptake appears to proceed in an energy-dependent fashion, since minimal cellular association occurred at 4 °C but it significantly increased at 37 °C even without any difference in nanoparticle–cell association between PMA and PEG-PMA nanoparticles. To gain more insight into the intracellular localization of the nanoparticles by DCs, we used stochastic optical reconstruction microscopy (STORM), a super-resolution microscopy technique that allows sub-diffraction-limited features to be resolved.[21] Figure 2C and D show a whole DC and part of a DC, respectively, whereas Figure 2E depicts a series of relevant events during the internalization process of the nanoparticles. These pictures show at high resolution the engulfment of the nanoparticles by the plasma membrane (Figure 2E1), lipid raft-mediated routing (Figure 2E2) and finally storage of the nanoparticles in endo/lysosomal vesicles (Figure 2E3). The most striking feature of these images is that they enable imaging at single-particle and single-endo/phago/lysosome resolution. CTB specifically binds to the ganglioside G_{M1} that is present on the plasma membrane of DCs, in particular at sites that are involved in lipid raft-mediated endocytosis.[20] In this case, it also provides an avenue for labeling lipid rafts and becomes incorporated in endo/lysosomal membranes, as shown in Figure 2E. This set of data is, to the best of our knowledge, amongst the first showing the potential of super-resolution microscopy for assessing the intracellular fate of nanoparticles. Note that trafficking of antigen in intracellular vesicles does not hamper efficient antigen presentation.[22]

Although PEGylation does not affect the uptake of 200 nm sized PMA and PEG-PMA nanoparticles by DCs in vitro, it might significantly enhance their mobility and lymph node drainage behavior in vivo. To address this,

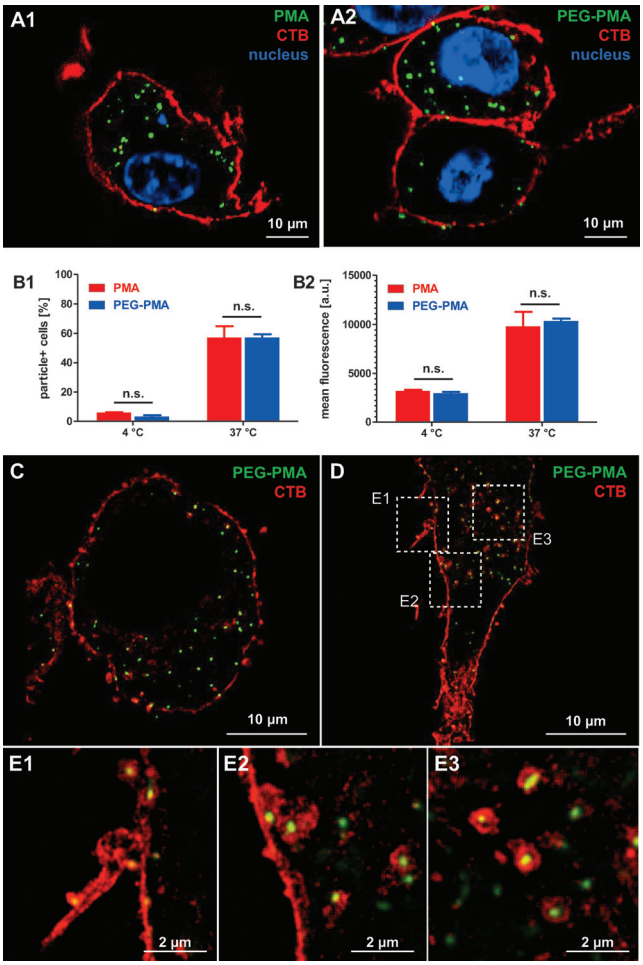

Figure 2. In vitro uptake of nanoparticles by DCs. A) Confocal microscopy and B) flow cytometry data of DCs pulsed with PMA^{SH} and PEG-PMA nanoparticles ($n=3$) ($p<0{,}001$: ***). C–E) STORM data of PEG-PMA nanoparticles internalized by DCs. Panels (E1–3) highlight different stages during the internalization process of the nanoparticles: E1) Engulfment of nanoparticles by the plasma membrane. E2) Intracellular routing and E3) storage in endo/lysosomal vesicles. In all panels particles are labelled with AF488 and the cell membrane is stained by AF647-CTB. In panels (A1–2), cell nuclei were stained with Hoechst.

AF488-labeled nanoparticles were injected subcutaneously into the footpad of mice followed by flow cytometry (FACS) analysis (gating strategy is depicted in Figure S3) of the draining lymph nodes at 12 and 48 h, post injection. Importantly, we noticed that neither PMA nor PEG-PMA nanoparticles induced significant swelling of the lymph nodes, which gives proof of their non-inflammatory nature. B cells were identified as CD3− and CD19+ cells. Lymph node macrophages were determined as CD3−, CD19−, CD64+, and CD11b+ cells. DCs were defined as CD3−, CD19−, CD11c+, and MHCII+ cells. Based on their relative expression of MHCII and CD11c, lymph node DCs were subdivided into migratory DCs ($CD11c^{int}$ $MHCII^{hi}$) and lymph node-resident DCs ($CD11c^{hi}$ $MHCII^{int}$).[12,23] Migratory DCs in lymph nodes represent tissue DCs that have migrated from peripheral tissue to the lymph nodes, while lymph node-resident DCs have spent their life cycle in the lymph nodes without prior presence in peripheral sites.

Within these respective populations, we determined the percentage of nanoparticle-associated cells and the intensity of the AF488 fluorescence signal within the particle positive population. Flow cytometry graphs of particle uptake are shown in Figure S4. The corresponding quantitative analysis (Figure 3A) proves that significantly higher percentages of B cells, macrophages, migratory DCs and lymph node-resident DCs were associated with PEG-PMA nanoparticles compared to PMA nanoparticles at 12 and 48 h post injection

On a cell-per-cell basis, the number of particles strongly increased in the case of PEG-PMA nanoparticles. At the DC level, migratory DCs associated more nanoparticles on a cell-per-cell basis when compared to resident DCs. This indicates that active transport of nanoparticles by DCs from the skin is an important mediator of both PEG-PMA and PMA nanoparticle drainage. Nevertheless, nanoparticles were also strongly present in non-migratory lymph node cells including macrophages, B cells, and lymph node-resident DCs, which suggests passive drainage of the nanoparticles also occurs. To further characterize the lymph node drainage properties of the nanoparticles, we analyzed their intranodal distribution. As can be seen from Figure 3B, higher numbers of PEG-PMA nanoparticles were present in the lymph nodes compared to PMA nanoparticles, confirming the FACS data. The majority of the nanoparticles were seen in the subcapsular sinus that lines the lymph nodes and in the B cell zone lying immediately beneath. The subcapsular sinus is the port of entry for all particles draining from the tissue, being either as free flowing particles or particles actively transported inside migratory DCs. The subcapsular sinus contains vast amounts of macrophages that capture free particles that arrive through the afferent lymph and transport the particles to B cells in the follicles beneath the capsular floor. Indeed, as shown in Figure 3C, many PEG-PMA nanoparticles are located at the border region between the subcapsular sinus and the B cell follicles, which also explains their high association with macrophages and B cells in FACS analysis. Importantly, nanoparticles were also visible in the deeper paracortex areas of the lymph node, where they are in the close presence of T cells (dashed rectangles in Figure 3C). Confocal microscopy images of sorted DCs and B cells (Figure 3D) also confirm internalization of the nanoparticles by these immune cell subsets.

Particles transported by migratory DCs have been reported to mostly end up in DCs in the T cell areas of the draining lymph nodes. Particles transported through active and passive transport show a wider cellular and subanatomical distribution pattern in the lymph node, reaching B cell follicles in addition to T cell areas. As a consequence, the intranodal distribution of the PEG-PMA nanoparticles, their presence in B cells, resident DCs and macrophages alongside with their high numbers in the migratory DC population strongly suggest that PEG-PMA nanoparticles drain to the lymph nodes through both active transport and passive lymphatic flow. PEGylation enforces both routes of transportation and our data demonstrate that PEGylation dramatically improves the lymph node targeting properties of

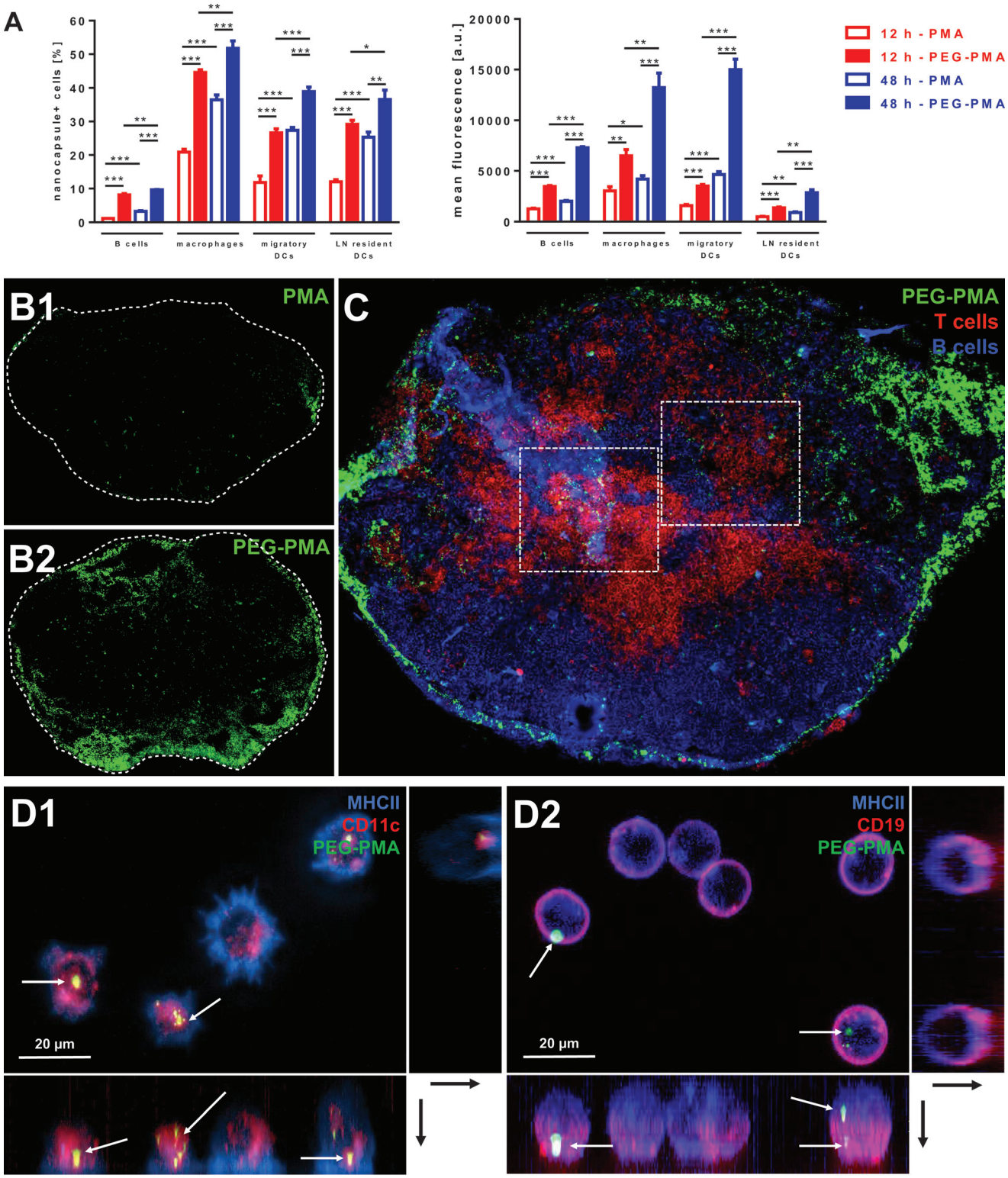

Figure 3. In vivo lymphatic transportation of nanoparticles. A) FACS analysis of particle-associated cells in the draining lymph nodes after subcutaneous injection of nanoparticles. ($n=3$; ***: $p<0.001$, **: $p<0.01$, *: $p<0.05$) B) Fluorescence microscopy of lymph nodes of mice injected with (B1) PMA and (B2) PEG-PMA nanoparticles, respectively. The dashed white lines are drawn to distinguish the contours of the lymph nodes. C) Fluorescence microscopy of lymph nodes of mice injected with PEG-PMA nanoparticles. Counterstaining was performed for T and B cell zones. D) Confocal microscopy (maximum intensity projection and orthogonal planes) of (D1) DCs and (D2) B cells sorted from lymph nodes of mice injected with PEG-PMA nanoparticles. The white arrows highlight nanoparticles.

PMA nanoparticles. Most likely, this can be attributed to the decreased fouling behavior of PEG-PMA versus non-PEGylated PMA nanoparticles. PMA^{SH}-based capsules have been reported to strongly interact with cysteine residues of proteins present on the cell surface.[24] In the present work, blocking the residual-free thiol and pyridyldisulfide groups of the nanoparticles by PEGylation reduces the interaction of PMA nanoparticles with the extracellular matrix and thereby dramatically improves their lymphatic transportation.

Finally, we investigated whether the increased lymph trafficking behavior of PEG-PMA nanoparticles translates into superior antigen presentation to T cells in the lymph nodes. Therefore, we conjugated the MHCI epitope (SIINFEKL) of the model antigen ovalbumin (OVA) to both PMA and PEG-PMA nanoparticles. This was performed by conjugating the cysteine-terminated peptide (i.e., CSIINFEKL) to PMA^{PDA} by thiol–disulfide exchange, followed by nanoparticle fabrication. Mice were immunized with the peptide-loaded nanoparticles and antigen presentation was assessed by measuring the proliferation of adoptively transferred, CFSE-labeled transgenic OVA-specific OT-I T cells in the draining lymph nodes. OT-I T cells are transgenic CD8 T cells with a T cell receptor that specifically recognizes the SIINFEKL epitope of OVA. FACS (gating strategy is given in Figure S5) can easily trace the number of OT-I divisions as the CFSE fluorescence signal halves each time the T cell divides. As shown in Figure 4, PEG-PMA nanoparticles evoked significantly more OT-I proliferation when compared to their non-PEGylated peptide bearing counterparts. This clearly demonstrates that delivery of the peptide by the PEGylated particles results in increased antigen presentation and augmented T cell priming.

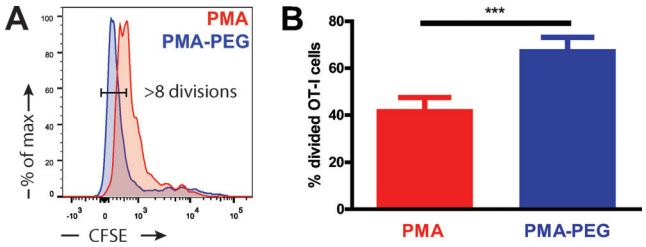

Figure 4. In vivo CD8 T cell response measured by quantifying the extent of proliferation of antigen-specific CD8 T cells in the spleen of mice that were immunized with either PEG-PMA or PMA nanoparticles. A) FACS histograms and B) corresponding percentage of antigen-specific CD8 T cells that underwent more than eight divisions. ($n = 3$; ***: $p < 0.001$).

In summary, we have demonstrated that PEGylation strongly improved lymph node targeting of hydrogel nanoparticles. More lymph node DCs and B cells became particle positive and the number of particles on a cell per cell basis increased dramatically, especially within the migratory DCs that originate from the injection site. This increased presence of particles in the lymph nodes resulted in increased priming of antigen-specific T cells. Although we did not analyze the humoral immune response—peptides are known to be poor inducers of antibody responses—this feature is likely to improve B cell activation by increased triggering of the cell surface B cell receptor and thus to lead to improved antibody responses to vaccination. Finally, in addition to the delivery of antigens, PEGylation of PMA nanoparticles also holds potential to improve the delivery of molecular adjuvants and drugs to the lymph nodes.

Acknowledgements

This research was conducted and funded by the Australian Research Council Centre of Excellence in Convergent Bio-Nano Science and Technology (project number CE140100036) and supported by the Australian Research Council under the Australian Laureate Fellowship (F.C., FL120100030). Dr. Ken Rock (University of Massachusetts Medical School) is gratefully acknowledged for providing the DC2.4 cell line. S.D.K. and B.G.D.G. acknowledge the FWO Flanders for funding. N.V. acknowledges BOF-UGent for a PhD scholarship.

Keywords: dendritic cells · disulfides · hydrogels · nanoparticles · vaccines

How to cite: *Angew. Chem. Int. Ed.* **2016**, *55*, 1334–1339
Angew. Chem. **2016**, *128*, 1356–1361

[1] J. J. Moon, B. Huang, D. J. Irvine, *Adv. Mater.* **2012**, *24*, 3724–3746.
[2] J. A. Hubbell, S. N. Thomas, M. A. Swartz, *Nature* **2009**, *462*, 449–460.
[3] S. De Koker, B. N. Lambrecht, M. A. Willart, Y. van Kooyk, J. Grooten, C. Vervaet, J. P. Remon, B. G. De Geest, *Chem. Soc. Rev.* **2011**, *40*, 320–339.
[4] B. G. De Geest, M. A. Willart, B. N. Lambrecht, C. Pollard, C. Vervaet, J. P. Remon, J. Grooten, S. De Koker, *Angew. Chem. Int. Ed.* **2012**, *51*, 3862–3866; *Angew. Chem.* **2012**, *124*, 3928–3932.
[5] M. Dierendonck, K. Fierens, R. De Rycke, L. Lybaert, S. Maji, Z. Zhang, Q. Zhang, R. Hoogenboom, B. N. Lambrecht, J. Grooten et al., *Adv. Funct. Mater.* **2014**, *24*, 4634–4644.
[6] B. G. De Geest, M. A. Willart, H. Hammad, B. N. Lambrecht, C. Pollard, P. Bogaert, M. De Filette, X. Saelens, C. Vervaet, J. P. Remon et al., *ACS Nano* **2012**, 2136–2149.
[7] S. P. Kasturi, I. Skountzou, R. A. Albrecht, D. Koutsonanos, T. Hua, H. I. Nakaya, R. Ravindran, S. Stewart, M. Alam, M. Kwissa et al., *Nature* **2011**, *470*, 543–547.
[8] C. M. Jewell, S. C. Bustamante Lopez, D. J. Irvine, *Proc. Natl. Acad. Sci. USA* **2011**, *108*, 15745–15750.
[9] J. J. Moon, H. Suh, A. Bershteyn, M. T. Stephan, H. Liu, B. Huang, M. Sohail, S. Luo, S. Ho Um, H. Khant et al., *Nat. Mater.* **2011**, *10*, 243–251.
[10] H. Liu, K. D. Moynihan, Y. Zheng, G. L. Szeto, A. V. Li, B. Huang, D. S. Van Egeren, C. Park, D. J. Irvine, *Nature* **2014**, *507*, 519–522.
[11] S. T. Reddy, A. J. van der Vlies, E. Simeoni, C. P. O'Neil, M. a. Swartz, J. a. Hubbell, *Eur. Cells Mater.* **2007**, *14*, 103.
[12] G. J. Randolph, V. Angeli, M. A. Swartz, *Nat. Rev. Immunol.* **2005**, *5*, 617–628.
[13] E. J. Wherry, M. Kurachi, *Nat. Rev. Immunol.* **2015**, *15*, 486–499.
[14] Y. Hailemichael, Z. Dai, N. Jaffarzad, Y. Ye, M. A. Medina, X.-F. Huang, S. M. Dorta-Estremera, N. R. Greeley, G. Nitti, W. Peng et al., *Nat. Med.* **2013**, *19*, 465–472.

[15] S. Kim, Y. T. Lim, E. G. Soltesz, A. M. De Grand, J. Lee, A. Nakayama, J. A. Parker, T. Mihaljevic, R. G. Laurence, D. M. Dor et al., *Nat. Biotechnol.* **2004**, *22*, 93 – 97.
[16] J. M. Harris, R. B. Chess, *Nat. Rev. Drug Discovery* **2003**, *2*, 214 – 221.
[17] J. Cui, Y. Yan, Y. Wang, F. Caruso, *Adv. Funct. Mater.* **2012**, *22*, 4718 – 4723.
[18] J. Cui, R. De Rose, K. Alt, S. Alcantara, B. M. Paterson, K. Liang, M. Hu, J. J. Richardson, Y. Yan, C. M. Jeffery et al., *ACS Nano* **2015**, *9*, 1571 – 1580.
[19] J. Cui, R. De Rose, J. P. Best, A. P. R. Johnston, S. Alcantara, K. Liang, G. K. Such, S. J. Kent, F. Caruso, *Adv. Mater.* **2013**, *25*, 3468 – 3472.
[20] N. Blank, M. Schiller, S. Krienke, G. Wabnitz, A. D. Ho, H.-M. Lorenz, *Immunol. Cell Biol.* **2007**, *85*, 378 – 382.
[21] M. J. Rust, M. Bates, X. Zhuang, *Nat. Methods* **2006**, *3*, 793 – 796.
[22] M. Houde, S. Bertholet, E. Gagnon, S. Brunet, G. Goyette, A. Laplante, M. F. Princiotta, P. Thibault, D. Sack, M. Desjardins, *Nature* **2003**, *425*, 402 – 406.
[23] L. Ziegler-heitbrock, P. Ancuta, S. Crowe, M. Dalod, V. Grau, N. Derek, P. J. M. Leenen, Y. Liu, G. Macpherson, G. J. Randolph et al., *Blood* **2014**, *116*, 5 – 7.
[24] Y. Yan, Y. Wang, J. K. Heath, E. C. Nice, F. Caruso, *Adv. Mater.* **2011**, *23*, 3916 – 3921.

Received: September 15, 2015
Revised: October 21, 2015
Published online: December 15, 2015

